The Tetrafluoro Analogue of DMABN: Anomalous Fluorescence and Mechanistic Considerations

Sukumaran Murali,[†] Vladimir Kharlanov,[†] and Wolfgang Rettig*[,†]

Institut für Chemie, Humboldt-Universität zu Berlin, Brook-Taylor-strasse 2, D-12489 Berlin, Germany

Alexei I. Tolmachev[‡] and A. V. Kropachev[‡]

Institute for Organic Chemistry of the National Academy of Sciences of Ukraine, Murmanskaya 5, Kiev-94, 02094, Ukraine

Received: February 10, 2005; In Final Form: May 30, 2005

Absorption and emission properties of DMABN-F4, the tetrafluoro analogue of DMABN, have been investigated and compared with the parent compound. Unlike in DMABN, this new compound exhibits only a highly solvatochromic and strongly red-shifted charge transfer (CT) fluorescence and is characterized by the absence of an LE band even in nonpolar solvents. This evidences the faster formation of CT in the excited state as compared to DMABN. The low quantum yield values of DMABN-F4 suggest that the high rate of nonradiative decay takes place via internal conversion (IC) rather than intersystem crossing (ISC) as no phosphorescence is observed in rigid glass solvents at 77 K in contrast to DMABN. The emission transition moment and radiative rate constant values of DMABN-F4 in medium and highly polar solvents point to a forbidden emission in the excited state similar to that of DMABN. Electronic structure and twist potentials were also studied by quantum chemical calculations using ab initio and semiempirical methods. In contrast to DMABN, the dimethylamino group in DMABN-F4 is found to be twisted by around 30−50°, but the photophysics are concluded to be analogous to DMABN with the addition of a very fast IC channel.

1. Introduction

Donor−acceptor-substituted benzenes have been the focus for many years regarding the nature of dual fluorescence or of emissions with very large Stokes shifts. Lippert et al.[1] showed that DMABN emits a dual fluorescence consisting of two bands assigned to two different excited states: The A band for the "anomalous" emission from the ^1L_a-type/charge transfer (CT) state, B band for the normal short wavelength arises from the ^1L_b-type state. The emitting species, also called A* and B* states, can be in thermal equilibrium.[5]

The photophysics of electron donor−acceptor aromatic systems has been well explained with the help of the twisted intramolecular charge transfer (TICT) model. According to this model,[2−5] the untwisted dimethylamino group (electron donor) rotates after photoexcitation toward an orthogonal orientation of the donor group relative to the aromatic ring system. In nonpolar solvents and under jet-cooled conditions, DMABN emits nearly exclusively from the planar LE excited state,[6] whereas a second minimum at a twisted conformation is populated on the excited-state energy surface in more polar solvents.

Recently, the effect of F-substitution in DMABN derivatives has been investigated for 4-(azetidinyl)benzonitrile by Druzhinin et al.,[7] who stated that there is no indication of dual fluorescence in alkane solvents for the fluoro derivatives of this molecule and that internal conversion is enhanced by the fluoro substituent.

CHART 1: Structures of the Molecules Investigated

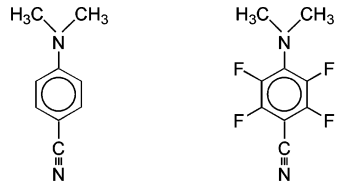

DMABN **DMABN-F4**

DMABN-F4, which differs more from DMABN by the increased strength of the acceptor unit, leads to the expectation of a lowering of the energy of the CT state, and therefore a red-shifted CT emission is expected. In the present publication, DMABN-F4 is characterized spectroscopically and compared with DMABN. The investigation of the spectroscopic behavior includes both polarity and temperature effects. The red shift of both absorption and stronger fluorescence spectra can be ascribed to this increase of the acceptor nature quantifiable by a more negative value of the electron affinity (EA).

To compare and interpret the spectroscopic properties, quantum chemical calculations were performed using ab initio and semiempirical methods.

2. Experimental Section

2.1. Materials. The compounds with their structures and abbreviations are shown in Chart 1. DMABN-F4 was synthesized by the reaction of pentafluorobenzonitrile with dimethylformamide using the procedure described in ref 8. The mp = 47−48 °C (in accordance with the literature value[8]). ^{19}F NMR spectrum: δ −137.0 ppm, 2F, doublet; −151.1 ppm, 2F,

* Corresponding author. E-mail: Rettig@chemie.hu-berlin.de.
† Humboldt-Universität zu Berlin.
‡ National Academy of Sciences of Ukraine.

10.1021/jp050726n CCC: $30.25
Published on Web 07/02/2005

doublet. Both these data are in accordance with the values reported in the literature,[8] if the NMR is recalculated from the standard C_6F_6 to CCl_3F.

^{1}H NMR spectrum: δ 3.08 ppm, 6H, triplet; $^2J_H-H = 3$ Hz. DMABN was a sample previously used. The absence of possible traces of impurities was confirmed by thin-layer chromatography (TLC). All the solvents for fluorescence spectroscopy were of Merck Uvasol quality.

2.2. Apparatus and Methods. Absorption spectra were measured on an ATI UNICAM UV series spectrometer UV4-021113. An AMINCO-Bowmann series 2 luminescence spectrometer was used for the measurement of corrected fluorescence spectra at room temperature (298 K). The measured fluorescence spectra were checked for impurity emission by exciting at different wavelengths of the absorption spectrum, and the emission maxima were found to be independent of excitation wavelengths and concentration variation.

Fluorescence quantum yields were determined relative to quinine bisulfate in 0.05 M H_2SO_4 ($\phi_f = 0.515$)[9] and corrected for the refractive index of the solvents. The determination of low-temperature fluorescence quantum yields took into account the temperature dependence of the refractive index as well as the increasing solvent contraction (density increase) with decreasing temperature.[10]

Fluorescence decay times of aerated solutions were determined with the time-correlated single-photon counting (SPC) technique[11] with a setup using an argon ion laser-pumped, passively mode locked Ti:sapphire laser as the excitation source. The pulse duration is about 80 fs, and the repetition rate is 82 MHz. The excitation wavelength, 265 nm, was obtained by frequency tripling of the fundamental wavelength of about 800 nm. The fluorescence was detected by a cooled microchannel plate photomultiplier (MCP, Hamamatsu R 1564 U-01 at -30 °C) coupled to the emission monochromator (Oriel MS257) by means of quartz fiber optics. The instrument response function was obtained by detection of Rayleigh scattered light in pure solvents and had a width of 56 ps at the excitation wavelength. The entire operation of the equipment is described in detail elsewhere.[12] The decay times were fitted using the iterative reconvolution procedure (Marquardt algorithm), which allowed a time resolution down to 0.1 ns and a relative precession of 0.1 ns. The absorption of the compound has been checked after the lifetime measurements, and the compounds were found to be photostable under these conditions.

2.3. Calculational Details. Semiempirical calculations for the compounds **DMABN** and **DMABN-F4** were carried out with full geometry optimization and with a vibrational analysis of the optimized structures by the Newton algorithm using the AM1 program contained in the AMPAC 6.0 package.[13,14]

The study of equilibrium and transition-state structures for the compounds by ab initio calculations at Hartree−Fock theory (HF) and density functional theory (DFT) levels were realized with different basis sets (6-31G(d), 6-311++(d,p), cc-pVDZ, and D95(d,p)) using Gaussian 98.[15] Full optimization of the ground state including vibrational analysis was performed to detect stable minima and transition geometries. The twist angle between the compound fragments was determined as the torsional angle between the lone pair on the nitrogen atom and the benzene plane, calculated from the bisector of the bonds linking the nitrogen with the two methyl groups (see Chart 2). The study of the fragment rotation in the S_0 state was carried out by fixing the torsional angle of one carbon atom of the dimethylamino group optimizing all other geometrical parameters.

CHART 2: Planar, Equilibrium, and Perpendicular Structures of the Dimethylamino Group for DMABN-F4 in the Ground State (Top) and Determination of the Dimethylamino Group Twist Angle α and the Dimethylamino Group Pyramidalization Angle *β* (Bottom)[a]

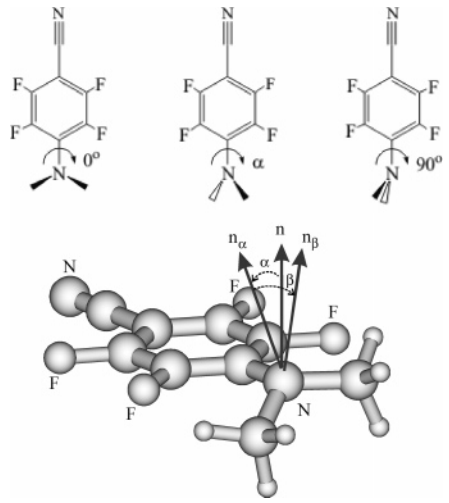

[a] n is a vector perpendicular to the plane of the aromatic ring, n_α is the bisector vector of the two *N*-methyl bonds of the dimethylamino group, and n_β is a vector perpendicular to the CNC plane of the dimethylamino group.

The calculations of the transition energies and oscillator strengths for the ground-state optimized geometries were carried out using configuration interaction (CI) for the optimized structures with inclusion of 10 unoccupied and 10 occupied orbitals (CI = 10) by ZINDO/s (CIS) included in Gaussian 98.

3. Results and Discussion

3.1. Absorption Spectra. The absorption spectra of DMABN-F4 in various solvents of different polarity are depicted in Figure 1a. The corresponding spectra of DMABN are also presented for comparison (Figure 1b). All spectra of DMABN-F4 as compared with the spectra of DMABN are shifted to the red (Table 1). In contrast to DMABN, in the spectrum of DMABN-F4 in hexane the weak shoulder is not visible, which is found at the red side of the main absorption maximum of DMABN and ascribed to absorption to the $^1L_b-S_1$ state. It can be concluded that the weak ^1L_b absorption band of DMABN-F4 is hidden by the stronger ^1L_a type band. It is even possible that the ^1L_a state is S_1 in this compound.

The molar extinction coefficient values for both compounds determined in this work in *n*-hexane are approximately equal [ϵ (λ_{282}^{max}) = 28 911 and ϵ (λ_{300}^{max}) = 34 436, respectively, for DMABN and DMABN-F4]. In view of the twisted ground-state structure of DMABN-F4 (see section 3.6, Theoretical Results), this might indicate a different vibronic mixing of the two lowest singlet states, ^1L_a and ^1L_b, such that the usual cos^2 law[16] does not apply here.

Analogous to DMABN, the long wavelength absorption band of DMABN-F4 is shifted to the red by increasing the solvent polarity (Figure 1 and Tables 1 and 2).

3.2. Fluorescence at Room Temperature. In all solvents studied, DMABN-F4 possesses very weak fluorescence (quantum yield $\phi_f \leq 0.002$) with a broad emission band ($\Delta\nu_{1/2} > 6000$ cm^{-1}) shifted unusually far from the long wavelength absorption band (Stokes shift $\Delta\nu_{St} \geq 11\,000$ cm^{-1}) even in hexane (Table 1 and Figure 1a). In contrast, in the latter solvent

TABLE 1: Photophysical Parameters of DMABN-F4 in Various Solvents at Room Temperature

solvent[a,b]	λ_{abs}^{max} (nm)	λ_{flu}^{max} (nm)	$\Delta\nu_{St}$ (10^3 cm^{-1})	ϕ_f	k_r (10^6 s^{-1})[c]	k_{nr} (10^8 s^{-1})[d]	M_f (D)[e]
Hex	300	456	11.40	0.0006	2.22	37	0.53
BOB	302	490	12.70	0.0018	1.74	9.6	0.50
BCl	306	496	12.52	0.0016	1.34	8.4	0.45
ACN	308	537	20.86	0.0001	0.47	47	0.33

[a] Solvent abbreviations: Hex − *n*-hexane; BOB − di-*n*-butyl ether; BCl − *n*-butyl chloride; ACN − acetonitrile. [b] The fluorescence maxima for further solvents are chloroform (485 nm), diethyl ether (501 nm) tetrahydrofuran (504 nm), ethyl acetate (512 nm), and ethanol (504 nm). [c] $k_r = \phi_f/\tau_f$. [d] $k_{nr} = k_r(\phi_f^{-1} - 1)$. [e] $M_f = \sqrt{3hk_r/64\pi^4 n^3 \nu_f^3}$.

TABLE 2: Photophysical Parameters of DMABN in Various Solvents at Room Temperature

				present work				
solvent[a]	λ_{abs}^{max} (nm)	λ_{flu}^{max} (nm)	$\Delta\nu_{St}$ (10^3 cm^{-1})	ϕ_f	ϕ_{tot}	ϕ_a/ϕ_b	ϕ_{tot}	ϕ_a/ϕ_b (lit)
Hex	282	341	6.14	0.16	0.16	0	0.11,[b] 0.18[c]	−
BCl	288	349 (B)	6.06 (B)	0.065 (B)	0.12	0.82	0.09[d]	0.8[e]
		390 (A)	9.08 (A)	0.053 (A)				
ACN	292	365 (B)	6.85 (B)	0.0016 (B)	0.02	10.12	0.02[b]	−
		476 (A)	13.24 (A)	0.0162 (A)				

[a] Solvent abbreviations: Hex − *n*-hexane; BCl − *n*-butyl chloride; ACN − acetonitrile. The quantum yield ratios in column 7 have been calculated on the basis of log-normal banshapes. [b] Rettig, W.; Bliss, B.; Dirnberger, K. *Chem. Phys. Lett.* **1999**, *305*, 8. [c] Demeter, A.; Druzhinin, S.; George, M.; Haselbach, E.; Roulin, J. L.; Zachariasse, K. A. *Chem. Phys. Lett.* **2000**, *323*, 351. [d] Rettig, W.; Wermuth, G.; Lippert, E. *Ber. Bunsen Phys. Chem.* **1979**, *83*, 692. [e] Rotkiewicz, K.; Köhler, G. *J. Lumin.* **1987**, *37*, 219.

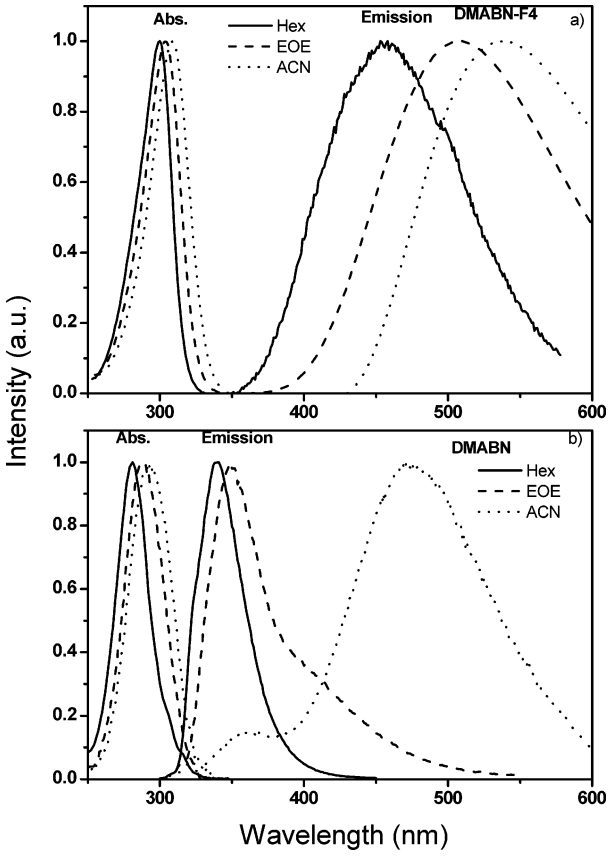

Figure 1. Absorption and normalized fluorescence spectra at room temperature of DMABN-F4 (a) and DMABN (b) in various solvents of different polarity. Hex = *n*-hexane; EOE = diethyl ether; ACN = acetonitrile.

the emission of DMABN is relatively strong ($\phi_f = 0.16$) and narrow (Figure 1b and Table 2). The absence of dual fluorescence and the indicated fluorescence properties (strong red shift) suggest a very fast formation of an emitting CT species in the excited singlet state of DMABN-F4 in contrast to DMABN. As one can see from Table 1, quantum yield values decrease from low-polarity to high-polarity solvents with the exception of hexane, where an anomalously high k_{nr} is found.

The fluorescence decay curves measured for DMABN-F4 in different solvents are monoexponential within the precision of our experiment and similar for different wavelengths of the emission spectra with the fluorescence lifetime ranging between 0.21 and 1.19 ns (Table 1). These measurements together with the spectra support the formation of only one long-lived emitting species in all solvents.

If we assume that the emitting species is populated without losses, then the radiative k_r and nonradiative k_{nr} rate constants can be calculated according to eqs 1 and 2:

$$k_r = \phi_f/\tau_f \tag{1}$$

$$k_{nr}^{tot} = k_r(\phi_f^{-1} - 1) \tag{2}$$

where k_{nr}^{tot} corresponds to the sum of all nonradiative processes, including triplet formation, internal conversion, and the possible formation of nonemissive photochemical products. The k_r values are extremely small and decrease from about 2×10^6 s^{-1} (the corresponding radiative lifetime τ_r is 450 ns) in hexane to 0.5×10^6 s^{-1} (τ_r is 2100 ns) (Table 3) in acetonitrile. Similarly, low k_r values were observed for a sterically hindered DMABN analogue, TMABN,[17,18] in which two methyl groups are present in ortho positions of the DMABN in the highly polar solvent propanol (5.1×10^6 s^{-1}). This gives supporting evidence for the forbidden radiative transition from the excited state, which is typical for TICT states.[5]

The formation of full charge transfer (i.e., a TICT state) in DMABN-F4 has been recently confirmed by time-resolved absorption spectroscopy.[19] The transient absorption spectrum in acetonitrile at 1-ps delay showed a band around 360 nm. It was attributed to the CT state by its similarity with that reported for DMABN at 100 ps. The much faster appearance time of the CT state of DMABN-F4 suggests that the CT formation is connected with a very small or even zero activation barrier in both polar and nonpolar solvents in this molecule and that TICT state formation is strongly favored with respect to DMABN.

The radiative transition moment values M_f in Table 3 as calculated from eq 3 decrease from hexane to acetonitrile in

TABLE 3: Photophysical Parameters (Radiative Lifetime τ_f, Radiative k_r, and Nonradiative k_{nr} Rate Constants, the CT Transition Dipole Moment, M_f) of DMABN-F4 and DMABN in Various Solvents at Room Temperature

	DMABN-F4				DMABN			
solvent	τ_f (ns)	k_r (10^6 s^{-1})	M_f (D)	k_{nr} (10^8 s^{-1})	τ_f (ns)[a]	k_r (10^6 s^{-1})	M_f (D)	k_{nr} (10^8 s^{-1})
Hex	0.27	2.22	0.53	37	2.3	48[a]	1.53[d]	3.9[a]
BOB	1.03	1.74	0.50	9.6		–	–	–
BCl	1.19	1.34	0.45	8.4		13.6[b,c]	0.96	–
ACN	0.21	0.47	0.33	47	3.0	7[a]	1.12[e]	3.3[a]

[a] Rettig, W.; Bliss, B.; Dirnberger, K. *Chem. Phys. Lett.* **1999**, *305*, 8−14. [b] Rettig, W. *J. Lumin.* **1980**, *26*, 21. [c] Van der Auweraer, M.; Grabowski, Z. R.; Rettig, W. *J. Phys. Chem.* **1991**, *95*, 2083. [d] Corresponds to the LE state. [e] Okada, T.; Uesugi, M.; Kohler, G.; Rechthaler, K.; Rotkiewicz, K.; Rettig, W.; Grabner, G. *Chem. Phys.* **1999**, *241*, 327.

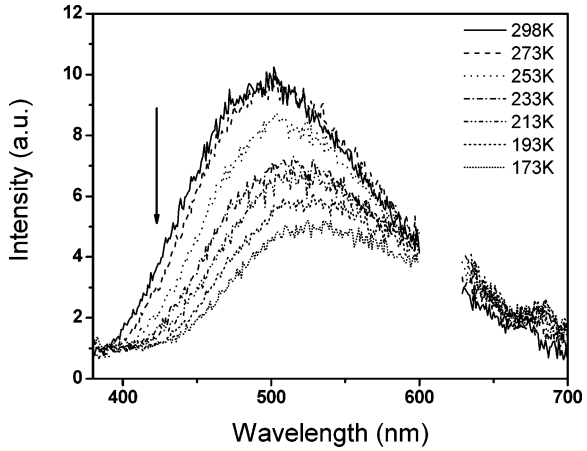

Figure 2. Low temperature effects on the fluorescence spectra of DMABN-F4 in *n*-butyl chloride. Down head arrow indicates decreasing temperature. The data points in the range 600−630 were omitted (second-order of excitation wavelength).

the case of DMABN-F4 in contrast to DMABN and TMABN, where the M_f values are independent of polarity.[18,20] The small magnitude of M_f in DMABN-F4 is typical for the twisted structure of a TICT state. In the case of TMABN, the smaller values of M_f can be interpreted by sterical hindrance, which leads to a narrowing of the angular distribution around 90° as compared to the unhindered compound DMABN and therefore to more strongly forbidden emission. It is remarkable that M_f of DMABN-F4 in acetonitrile is the smallest value ever reported for the TICT fluorescence of an aniline derivative, lower even than that for TMABN or other twisted model compounds of DMABN.

$$M_f = \sqrt{3hk_r/64\pi^4 n^3 \nu_f^3} \qquad (3)$$

3.3. Fluorescence at Low Temperatures. The fluorescence study of DMABN-F4 at lower temperatures was done in *n*-butyl chloride to study the relaxation processes in a glassy matrix. These measurements detected a weak red shift of the emission maximum from 501 to 535 nm and a decrease of the fluorescence quantum yield by more than a factor of 2 when the solvent is cooled from room temperature to 173 K (Figures 2 and 3, Table 4). Further cooling until 77 K did not allow quantum yield measurements, but the fluorescence band is found to be weak and shifted to the blue by 35 nm. However, even with the rigid glass matrix at 77 K the LE emission and phosphorescence are absent. In contrast to this, DMABN at 77 K possesses only the LE emission at 342 nm, and a phosphorescence peak is observed at 411 nm with a highly structured band (Figure 3b). The red-shifted spectrum of DMABN-F4 at 77 K gives evidence that there is some relaxation even in a highly polar glassy matrix.

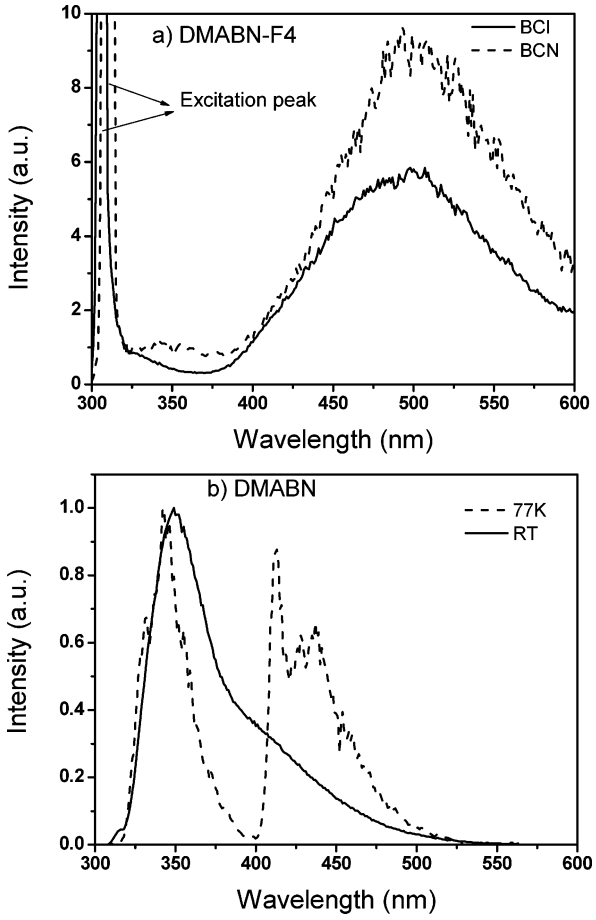

Figure 3. Fluorescence spectra of (a) DMABN-F4 in BCl (*n*-butylchloride) and BCN (*n*-butyronitrile) at 77 K and (b) DMABN in BCl at room temperature and at 77 K.

TABLE 4: Temperature Dependence of the Photophysical Data of DMABN-F4 in BCl

T (K)	λ_{flu}^{max} (nm)	ν_{flu} (cm^{-1})	$\Delta\nu_{1/2}$ (cm^{-1})	ϕ_f	τ_f (ns)	k_r (10^6 s^{-1})	k_{nr} (10^8 s^{-1})
298	501	19960	6320	0.0016	1.19	1.34	8.40
273	505	19802	6910	0.0014	1.20	1.25	8.32
253	510	19608	5730	0.0013	1.19	1.09	8.37
233	516	19380	5910	0.0011	1.15	0.96	8.71
213	521	19194	5850	0.0009	1.09	0.92	9.19
193	530	18868	6300	0.0007	0.99	0.81	10.1
173	535	18692	7100	0.0006	–	–	–

3.4. Geometry of the Ground State. The calculations indicate that, in contrast to planar DMABN, the derivative with fluorine atoms DMABN-F4 possesses a somewhat twisted equilibrium geometry in the ground state (torsional angle between the fragments is 35−50°, depending on the calculation method; see Figure 4 and Table 5). The reason is a stronger sterical interaction between the two methyl groups of $N(CH3)_2$

TABLE 5: Ground-State Characteristics of the Molecules Studied: Dipole Moment μ_{eq}, Equilibrium Twist Angle α_{eq}, Equilibrium Pyramidalization Angle β_{eq}, Activation Barrier of the Intramolecular Fragment Rotation to the Planar ($\Delta H(00)$), and the Perpendicular ($\Delta H(90)$) Geometry for DMABN-F4 and DMABN as Calculated by Different ab Initio and Semiempirical Methods and Different Basis Sets

compound	method	μ_{eq} (D)	α_{eq} (deg)	β_{eq} (deg)	$\Delta H(00)$ (kcal/mol)	$\Delta H(90)$ (kcal/mol)
DMABN-F4	AM1	4.62	29.34	10.84	1.35	2.52
	HF	6.64[a]	33.35	0.07	4.58	0.38[b]
		6.19[c]	51.99	29.56	5.36	0.50[b]
		5.97[d]	51.27	29.86	4.76	0.47[b]
		6.10[e]	53.29	31.98	5.41	0.30[b]
	DFT (Becke3LYP)	7.09[a]	33.70	0.87	3.09	3.32
		7.48[c]	35.09	0.01	3.76	3.23
		6.56[d]	38.18	11.55	2.87	3.05
		7.10[e]	40.09	20.78	3.15	3.08
	MP2	6.58[a]	40.86	0.00	4.27	–
DMABN	AM1	5.35	0.00	25.15	0.00	2.45
	HF	7.29[a]	0.00	14.85	0.00	2.09
	DFT (Becke3LYP)	7.63[a]	0.00	0.95	0.00	5.98
		7.87[f]	0.00	6.50	0.00	11.27
	MP2[g]	–	0.00[a]	28.8	–	–

[a] 6-31G(d) basis set. [b] Local minimum. [c] 6-311++G(d) basis set. [d] cc-pVDZ basis set. [e] D95(d,p) basis set. [f] TVZP basis set (Parusel, A. B. J. *Phys. Chem. Chem. Phys.* **2000**, *2*, 5545). [g] Sobolewski, A. L.; Sudholt, W.; Domcke, W. *J. Phys. Chem. A* **1998**, *102*, 2716.

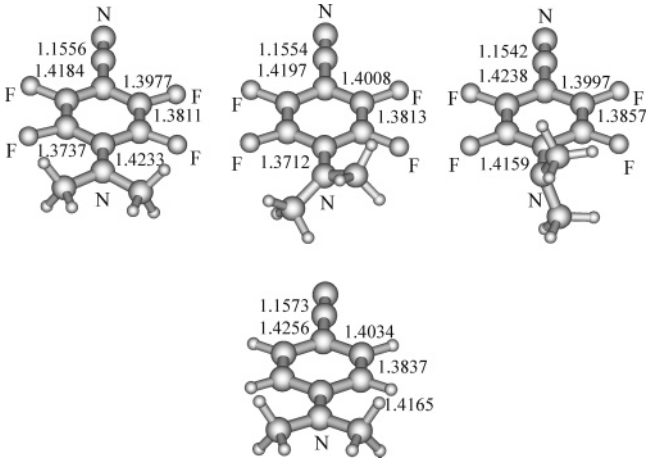

Figure 4. Planar transition, twisted equilibrium, and perpendicular transition structures of DMABN-F4 and the planar equilibrium geometry of DMABN with some geometrical characteristics calculated by DFT (B3LYP/6-311++G(d)).

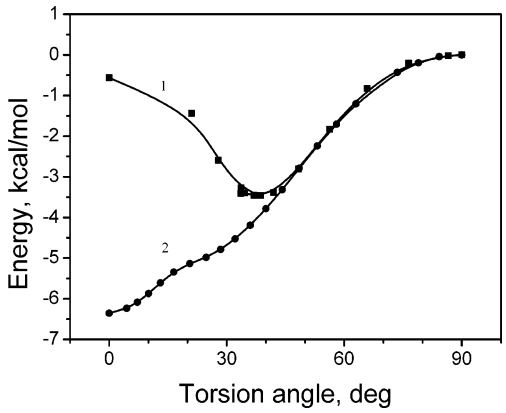

Figure 5. Ground-state potentials of DMABN-F4 (1) and of DMABN (2) calculated by DFT (B3LYP/6-31G(d)) method. The torsion angle is determined according to Chart 2. The inflection in the potential for DMABN at around 15° is due to different methyl group conformations being the most stable ones (see Chart3).

and the fluorine atoms in the benzene ring. The interaction is caused by the longer C−F bond (close to 1.3 Å for all calculation methods) in DMABN-F4 as compared to the C−H bond length close to 1.08 Å in DMABN. The pyramidalization of the dimethylamino group of DMABN-F4 is predicted very differently depending on basis set and method used. For the conditions of Figure 4, it is practically nonpyramidal in the equilibrium structure (near sp^2 hybridization). Similar strong variations of the pyramidalization depending on the method can be observed for DMABN (Table 5).

For comparable methods, both semiempirical and ab initio calculations demonstrate an sp^3 hybridization of the dimethylamino group for the relaxed geometries of DMABN-F4 smaller than those for DMABN (from AM1, equilibrium pyramidalization angles are around 13° and 29°, respectively; Table 5).

The intramolecular fragment rotation away from the equilibrium geometry to the planar and perpendicular geometries of DMABN-F4 (Table 5, Figure 5) increases the potential energy. Both planar and perpendicular geometries possess a C_s symmetry and correspond to a saddle point (Chart 2) (one negative Eigenvalue in the Hessian matrix).

TABLE 6: Relative Energy[a] (from DFT-B3LYP/6-31G(d) Calculations) in kcal/mol (Number of Negative Eigenvalues χ of the Hessian Matrix) and the Symmetry Point Group for Planar Arrangements of the Dimethylamino Group (Chart 3) of the Compounds DMABN and DMABN-F4

compound	syn1	syn2	syn3
DMABN	0.00 ($\chi = 0$) C_s	2.39 ($\chi = 2$) C_{2v}	1.39 ($\chi = 2$) C_s
DMABN-F4	0.00 ($\chi = 1$) C_s	1.54 ($\chi = 2$) C_{2v}	0.62 ($\chi = 2$) C_s

[a] Relative to the energies calculated for the nontwisted equilibrium (DMABN) and nontwisted transition geometries (syn1) (DMABN-F4), both slightly pyramidal.

A study of the possible conformations of the two methyl groups of the dimethylamino $N(CH3)_2$ fragment shows that several conformers are important (Chart 3) and that only conformer syn1 with C_s symmetry for the planar and twisted geometries has the lowest energy, and the Hessian matrix indicates a saddle point of first-order. The other conformers syn2 and syn3 of the symmetries C_{2v} and C_s possess saddle points of second-order (Table 6). Depending on the twist angle, the relative energy of the conformers can change. This is the reason for the inflection in the potential for DMABN at around 15° (Figure 5).

TABLE 7: Onsagar Radius, Solvatochromic Slope of the Mataga Plot, and Calculated Ground and Derived Excited-State Dipole Moments of DMABN and DMABN-F4

compound	a (Å)[a]	a (Å)[b]	a (Å)[c]	slope (10^3 cm^{-1})[f]	μ_g (D)	μ_e (D)[a]	μ_e (D)[b]	μ_e (D)[c]
DMABN	3.7	4.3	4.5[d]	6.3(B)	6.7[d]	9.9(B)	11.1(B)	11.6(B)
				24.2(A)		14.8(A)	17.6(A)	18.5(A)
DMABN-F4	3.8	4.5	4.5	8.4	6.2[e]	10.5	12.4	12.4

[a] From the mass densitiy formula, eq 5. [b] From the molecular volume as calculated using the HF method. [c] Based on Lippert approach of the long molecular axis in ref. Lippert, E. *Z. Naturforsch.* **1955**, *10a*, 541. [d] Baumann, W.; Bischof, H.; Froehling, J. C.; Brittinger, C.; Rettig, W.; Rotkiewicz, K. *J. Photochem. Photobiol., A* **1992**, *64*, 49. [e] Approximated from μ_g(DMABN) + $\Delta\mu_{cal}$(DMABN-F4 − DMABN). [f] Error estimated at less than 10%.

CHART 3: Possible Conformation of Methyl Group of Dimethylamino Group for DMABN-F4 and DMABN in the Ground State

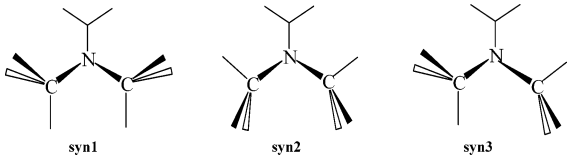

TABLE 8: Densities and Onsager Radius, Compared for Benzene, Fluorinated Benzenes, DMABN, and DMABN-F4

molecules	ρ[a] (g/cm^3)	a[b] (Å)	a[c] (Å)
benzene	0.877	3.28	4.00
F-benzene	1.022	3.34	3.92
1,2,-F-benzene	1.157	3.39	4.02
1,2,4,5-F-benzene	1.319	3.56	3.90
hexafluorobenzene	1.618	3.57	3.71
dimethylaminobenzene	0.956	3.82	4.23
DMABN	1.129[d]	3.72	4.28
DMABN-F4	1.561[e]	3.81	4.45

[a] *CRC Handbook of Chemistry and Physics*, 73rd ed.; Lide, D. R., Ed.; CRC Press: Boca Raton, FL, 1992−1993. [b] From eq 5: $a = \sqrt[3]{3M/4\pi N_A\rho}$. [c] The Onsager radii were determined by Gaussian 98 for the optimized equilibrium geometries using the HF/6-311G(d) method. [d] Heine, A.; Herbstirmer, R.; Stalke, D.; Kuhnle, W.; Zachariasse, K. A. *Acta Crystallogr.* **1994**, *B50*, 363. [e] Estimation using DMABN and the difference between 1,2,4,5-F-benzene and benzene.

3.5. Dipole Moment at Room Temperature. The excited-state dipole moments μ_e of DMABN-F4 and DMABN were determined from the solvatochromic slopes by applying the Mataga eq 4.[21] The slopes from the corresponding solvatochromic plots of the emission maxima against the solvent polarity parameter, $\Delta f'$, can be used to calculate the excited-state dipole moment. Different values result from different assumptions regarding the Onsager radius *a*. These are compiled in Table 7 for the cases where "*a*" was calculated from (1) the mass−density formula (eq 5),[22] (2) the molecular volume as calculated using the HF method, and (3) using the Lippert approach.[21] To gain a more reliable basis, the Onsager radii for different fluorosubstituted benzenes and dimethylaminobenzenes were determined from the experimental densities and the molecular weight (eq 5). As one can see from Table 8, addition of one or more fluorine atoms to benzene does not induce any drastic changes in the value of the Onsager radius. Thus, it is not surprising that both DMABN and DMABN-F4 are predicted to have similar Onsager radii. Hence, the three above-mentioned methods resulted in approximately the same excited-state dipole moment values for the CT state: around 13 D for DMABN-F4 and 18 D for DMABN. For the usual point dipole Onsager model, because of similar Onsager radii, the resulting significantly different CT dipole moment values are entirely a consequence of the difference of the experimental solvatochromic slopes.

$$\nu_f = -\frac{2\Delta f'}{4\pi \epsilon_0 hca^3}\mu_e(\mu_e - \mu_g) + \text{const} \qquad (4)$$

where $\Delta f' = (\epsilon - 1)/(2\epsilon + 1) - {}^1/_2(n^2 - 1)/(2n^2 + 1)$

$$a = \sqrt[3]{3M/4\pi N_A\rho} \qquad (5)$$

In the above equations, μ_e and μ_g are the excited- and ground-state dipole moments, respectively, h is Planck's constant, c is the velocity of light, M is the molecular mass, N_A is Avogadro's number, and n and ϵ are the refractive index and dielectric constant, respectively.

3.6. Theoretical Results. *3.6.1. Electronic Property of the Acceptor Fragments.* For the discussion of the CT structure and dipole moment, it became important to know more about the properties and relative energies of the acceptor orbitals involved. Although fluorine substitution is expected to lead to an overall lowering of the energy of the acceptor orbitals, a closer look into the reported literature shows that this lowering very strongly depends on the substitution pattern and that orbitals of different symmetry can exchange their energetic position. We therefore undertook to calculate the orbital energies of both the highest two occupied orbitals and the lowest two unoccupied orbitals by different methods and to compare them to the available experiments (Table 9). Especially useful is a look at their energetic difference (Table 10), which changes from negative to positive values if the orbitals exchange their energetic position. Both the theoretical and the experimental results (Table 9) show that inserting the fluorine atoms into the benzene ring increases the acceptor property of this fragment. The HF ab initio calculations (Table 9) for a series of compounds containing fluorine are in rather good agreement with the experimental ionization energies, but the electron affinities are poorly represented. On the other hand, DFT (B3LYP/6-31G(d)) shows a much better correspondence of EA to the LUMO energies than HF. Figure 6 shows that, depending on the substitution pattern and the number of fluorine atoms, the orbitals of different symmetry (labeled with respect to the C_2 symmetry point group) exchange their energetic position. Figure 7 depicts the HOMO and LUMO energies calculated with HF and DFT: HF fits much better to the experimental ionization energy, whereas the correspondence of DFT LUMO energies and the experimental electron affinities is much better. Both methods agree, however, in the prediction of the relative changes of orbital energies with the fluorine substitution pattern.

Figure 6 and Tables 9 and 10 show that, in some compounds (1-fluoro and 1,4-difluorobenzene), the orbitals of B symmetry are higher-lying than the orbitals of A symmetry. In the twisted geometry, the electron transfer from dimethylamino group (the donor orbital transforming as B) can be to either of the two lowest LUMO orbitals of the acceptor. This could have the

TABLE 9: Energies *E* of the Four Frontier Orbitals (the Orbital Symmetries within Point Group C_2), Calculated for Optimized Geometries of Benzene with Different Substituents (Fluorine Atom F and CN Group) and Comparison to the Negative Experimental Values of Ionization Potential I_e and the Electron Affinity EA[a]

"F" and other substituents	HF/6-31G(d) ϵ (MO) eV calcd	$-I_e$ eV[b] expt	DFT(B3L/6-31G(d)) ϵ (MO) eV calcd	$-$EA eV[c] expt	Δ EA (expt $-$ calcd)
0	4.07 (B)		0.10 (A)		
(F 0)	4.07 (A)		0.10 (B)	+1.15 [1,2]	1.0
	−9.00 (B)	−9.24	−6.70 (B)		
	−9.00 (A)	−9.24	−6.70 (A)		
1	4.12 (B)		0.10 (B)		
(F 1)	3.65 (A)		−0.24 (A)	+0.89 [1,2]	1.1
	−9.08 (B)	−9.19	−6.62 (B)		
	−9.45 (A)	−9.63	−7.04 (A)		
CN	3.29 (A)		−0.67 (A)		
(CN)	2.45 (B)		−1.41 (B)	+0.23 [3]	1.6
	−9.66 (B)	−	−7.26 (B)		
	−9.84 (A)		−7.52 (A)		
1,4	4.18 (B)		0.10 (B)		
(F 1,4)	3.21 (A)		−0.57 (A)	−	
	−9.16 (B)	−9.32	−6.56 (B)		
	−9.88 (A)	−9.68	−7.37 (A)		
1,3,5	3.59 (B)		−0.36 (B)		
(F 1,3,5)	3.59 (A)		−0.36 (A)	−	
	−9.79 (A)	−9.62	−7.09 (A)		
	−9.79 (B)	−9.62	−7.09 (B)		
1,2,4,5	3.81 (A)		−0.24 (A)		
(F 1,2,4,5)	2.90 (B)		−0.82 (B)	−	
	−9.60 (A)	−9.36	−6.78 (A)		
	−10.34 (B)	−10.04	−7.56 (B)		
1,2,3,4,5	3.42 (A)		−0.52 (A)		
(F 1,2,3,4,5)	2.95 (B)		−0.82 (B)	−0.64 [3]	0.2
	−9.99 (A)	−9.64	−7.06 (A)	−0.86 [4]	
	−10.35 (B)	−	−7.43 (B)		
1,2,3,4,5,6	3.02 (B)		−0.81 (A)		
(F 1,2,3,4,5,6)	3.02 (A)		−0.81 (B)	−0.52 [3]	0.3
	−10.36 (B)	−9.90	−7.33 (A)	−0.73 [4]	
	−10.36 (A)	−9.90	−7.33 (B)		
1,2,4,5,CN	3.13 (A)		−0.89 (A)		
(F1,2,4,5,CN)	1.41 (B)	−	−2.19 (B)	−	
	−10.28 (A)		−7.44 (A)		
	−10.80 (B)		−7.96 (B)		
1,2,3,4,5,CN	2.76 (A)		−1.17 (A)		
	1.45 (B)	−	−2.20 (B)	−1.08 [3]	1.1
	−10.68 (A)		−7.72 (A)		
	−10.79 (B)		−7.86 (B)		
DMABN-F4	3.40 (A)		−0.54 (A)[d]		
	1.98 (B)	−	−1.54 (B)[d]	−	
	−9.06 (B)		−6.16 (B)[d]		
	−10.10 (A)		−7.12 (A)[d]		

[a] F0 − benzene, F1 − fluorobenzene, CN − cyanobenzene, F 1,4 − 1,4-difluorobenzene, F 1,3,5 − 1,3,5-trifluorobenzene, F 1,2,4,5 − 1,2,4,5-tetrafluorobenzene, F 1,2,3,4,5 − 1,2,3,4,5-pentafluorobenzene, F 1,2,4,5,CN − 1,2,4,5-tetrafluorobenzonitrile. Symmetry designations A and B mean that orbitals with A symmetry have a zero orbital coefficient for the atoms lying on the C_2 twist axis, those with B symmetry have a nonzero coefficient for these orbitals and are symmetric with respect to a plane perpendicular to the molecular plane and containing the C_2 axis. [b] From Streets, D. G.; Caesar, G. P. *Mol. Phys*. **1973**, *26*, 1037; Duce, C. B.; Yip, K. L.; Caesar, G. P.; Potts, A. W.; Streets, D. G. *J. Chem. Phys*. **1977**, *66*, 256. [c] By electron transmission spectroscopy in the gas phase: (1) Jordan, K. D.; Michejda, J. A.; Burrow, P. D. *J. Am. Chem. Soc*. **1976**, *98*, 7189. (2) Jordan, K. D.; Burrow, P. D. *Acc. Chem. Res*. **1978**, *11*, 341. (3) Chowdhury, S.; Grimsrad, E. P.; Heinis, T.; Kebarle, P. *J. Am. Chem. Soc*. **1986**, *108*, 3630. (4) Wentworthm, W. E.; Limero, T.; Chen, C. M. *J. Phys. Chem.* **1987**, *91*, 241. [d] Local symmetry on the acceptor group.

consequence that also the energetic position of the two possible TICT states interchanges, and the lowest TICT state could become of B symmetry instead of A symmetry as in DMABN.

The results for 1,2,4,5-tetrafluorobenzene, however, clearly show that the B orbital is lower than the A orbital for both the HOMO and the LUMO manifold, and this effect is enhanced for the LUMO by introducing a further cyano group (but weakened for the occupied orbitals of the acceptor). From the DFT-LUMO energies for 1,2,4,5-tetrafluorbenzene and its cyano derivative (Table 9), we can conclude that the four fluorine atoms lower the LUMO energy by 0.78 eV.

Thus, we can conclude that the properties of the lowest TICT state should be the same for DMABN and DMABN-F4 regarding symmetry, and hence also the charge distribution should be similar.

This lowering of the TICT energy also has consequences for the reaction enthalpy of the B* → A* reaction. In the gas phase, it is calculated as being uphill (endothermic) for both com-

TABLE 10: Energy Difference $\Delta\epsilon$ (eV) = ϵ(B) − ϵ(A) of the Molecular Orbitals of Benzene with Different Substituents and with Different Symmetry as Calculated by the Following Methods: HF/6-31G(d), AM1, DFT (B3LYP/6-31G(d)), and Compared to Experimental Values as Far as Available[a]

position of F-substituents and other substituents	HF	AM1	DFT (B3LYP/6-31G(d)	expt[b]
0	0.00	0.00	0.00	
	0.00	0.00	0.00	
1	0.47	−0.06	0.34	−
	0.37	0.49	0.42	0.44
CN	−0.84	−0.46	−0.74	−
	0.18	0.15	0.26	−
1,4	0.97	−	0.67	−
	0.72	−	0.81	0.83
1,3,5	0.00	0.00	0.00	−
	0.00	0.00	0.00	0.00
1,2,4,5	−0.91	0.10	−0.58	−
	−0.74	−0.83	−0.78	−0.68
1,2,3,4,5	−0.47	−	−0.30	−
	−0.36	−	−0.37	−
1,2,3,4,5,6	0.00	0.00	0.00	−
	0.00	0.00	0.00	0.00
1,2,4,5,CN	−1.72	−0.26	−1.30	−
	−0.52	−0.68	−0.52	−
1,2,3,4,5,CN	−1.31	−	−1.03	−
	−0.11	−	−0.06	−

[a] Upper rows: difference of the first two LUMOs. Lower rows: difference of the two highest occupied orbitals. [b] Calculated from the negative experimental IP values in Streets, D. G.; Caesar, G. P. *Mol. Phys.* **1973**, *26*, 1037.

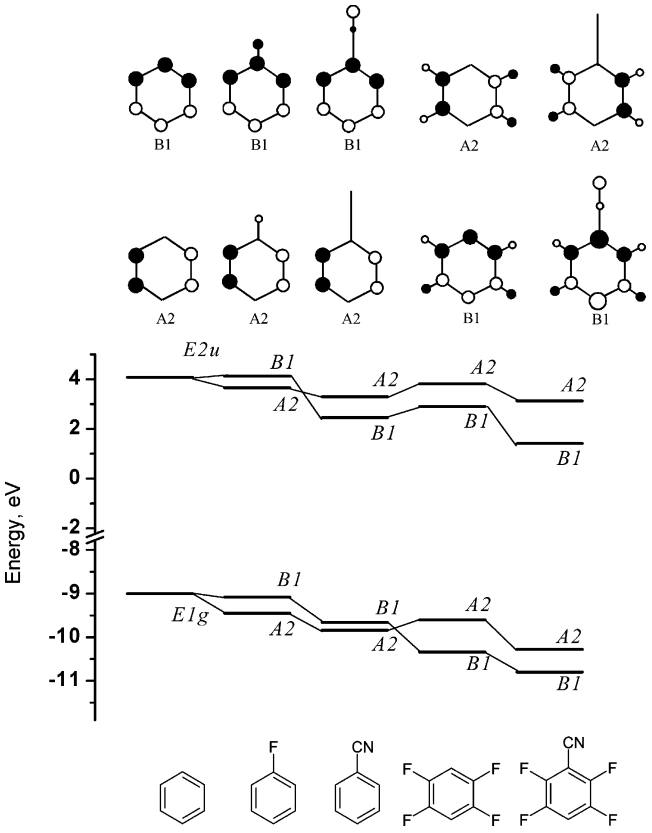

Figure 6. Correlation diagram of the energies of the occupied and unoccupied orbitals of fluorinated benzenes and benzonitrile as calculated by HF (for values, see Table 6).

pounds, but significantly less so for DMABN-F4. Thus, for a given solvent polarity, where the reaction is exothermic in DMABN, the exothermicity is much larger for DMABN-F4 (Chart 4).

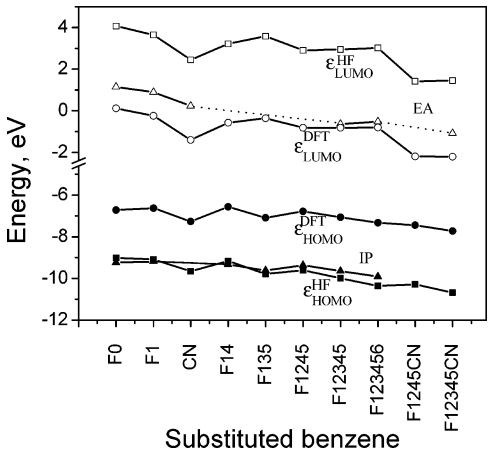

Figure 7. Comparison of the orbital energy for HOMO (ϵ_{homo}) and LUMO [(ϵ_{lumo}) calculated by different methods (HF/6-31G(d) and DFT (B3LYP/6-31G(d))] with the negative experimental values of electron affinity (EA) and ionization potential (IP) for different compounds. The compounds are defined in Table 6.

CHART 4: Schematic Diagram Showing the State Energies of DMABN and DMABN-F4 in the Gas Phase, as Calculated by ZINDO/s

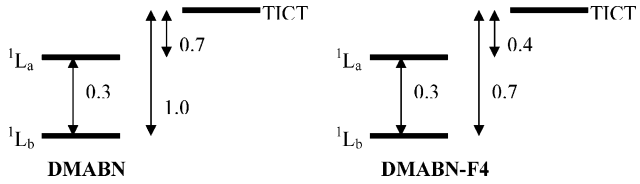

3.6.2. Electronic Transitions. The semiempirical ZINDO/s calculations show that the long wavelength absorption region of DMABN and DMABN-F4 consists of two transitions (Table 11). The position and intensity of these transitions are characterized by an allowed S_2 transition (4.22 eV, $f = 0.49$ and 4.59 eV, $f = 0.64$ for DMABN-F4 and DMABN, respectively) with CT nature (dipole moment 12.4 D similar to DMABN) and a polarization along the long molecular axis (^1L_a-type according to Platt nomenclature). Thus, there is a clear red shift of the ^1L_a-type state as expected from the increased acceptor strength also shown by the experimental spectra (Figure 1). The forbidden S_1 transition ($f = 0.01$) with a somewhat lower energy (3.93 eV in DMABN-F4) is of ^1L_b nature and does not lead to a structure in the absorption spectrum (Figure 1a), in contrast to the similar S_1 transition (4.27 eV, $f = 0.02$) of DMABN, which leads to a weak shoulder on the red side of the absorption spectrum. The absence of structure in the absorption spectrum of DMABN-F4 in hexane is in contrast to the calculated $S_1 - S_2$ energy difference (Table 11), which is even larger for DMABN-F4 (0.52 eV) than that for DMABN (0.32 eV). We consider that the energy lowering of the ^1L_b-type state in DMABN-F4 is probably smaller than predicted by the calculations in Table 11.

The stronger acceptor character of tetrafluorobenzonitrile as compared to that of benzonitrile is also reflected in the energy of the calculated (and observed) TICT state: In DMABN, it is calculated at 5.36 eV, in DMABN-F4 at 4.60 eV, that is, 0.76 eV lower, very close to the value predicted by the lowering of the LUMO orbital energy of the acceptor (0.78 eV, Table 9). As a consequence, in contrast to DMABN, the lowest TICT state of DMABN-F4 calculated for 90° corresponds to S_2, whereas it is S_4 in DMABN in the gas phase according to the ZINDO/s calculations.

TABLE 11: Comparison of the Transition Energy ΔE, Oscillator Strength F, Dipole Moments, and Configuration Interaction Analysis for the Long Wavelength Absorption Transitions for DMABN and DMABN-F4 as Calculated by ZINDO/s for the Optimized Ground-State Equilibrium Geometry and Two Further Twist Angles[a]

	DMABN twist angle and symmetry			DMABN-F4 twist angle and symmetry		
parameter	00_cs[eq]	35_c1[b]	90_cs	00_cs	35_c1[eq]	90_cs
ΔE ($S_0 \rightarrow S_1$), eV (f)	4.27 (0.02)	4.27 (0.02)	4.49 (0.00)	3.94 (0.01)	3.93 (0.01)	4.16 (0.00)
μ (S_1) (μ (S_0), D)	8.36 (7.34)	8.33 (7.04)	5.84 (5.94)	8.81 (7.48)	8.87 (7.10)	5.90 (5.85)
$\Delta\mu$, D	1.02	1.29	0.10	1.33	1.77	0.05
CI coefficient: HOMO+0 → LUMO+1	0.58	0.58	0.46	0.56	0.57	0.47
HOMO−1 → LUMO+0	0.38	0.39	0.52	−0.42	−0.40	−0.52
nature	^1L_b	^1L_b	LE(BN)[c]	^1L_b	^1L_b	LE(BN)[c]
ΔE ($S_0 \rightarrow S_2$), eV (f)	4.59 (0.64)	4.53 (0.56)	5.36 (0.00)	4.46 (0.57)	4.22 (0.49)	4.60 (0.00)
μ (S_2) (μ (S_0), D)	12.51 (7.34)	13.26 (7.04)	16.66 (5.94)	12.35 (7.48)	13.27 (7.10)	16.81 (5.85)
$\Delta\mu$, D	5.17	8.22	10.72	4.87	6.17	10.96
CI coefficient: HOMO+0 → LUMO+0	0.68	0.68	0.64	0.68	0.68	0.65
nature	L_a/CT	L_a/CT	TICT[d]	L_a/CT	L_a/CT	TICT[d]

[a] Full optimization at the different fixed twist angles using DFT (B3LYP/6-311++G(d). [b] Fixed torsional angles of the carbon atoms of the dimethylamino group which are equal to the equilibrium orientation of the group for DMABN-F4. [n] LE state localized on the benzonitrile moiety. [d] S_4 for DMABN, S_2 for DMABN-F4.

3.7. The Discrepancy of Experimental and Calculated CT Dipole Moments. On the basis of the solvatochromic measurements, the resulting CT dipole moments of DMABN (18 D) and DMABN-F4 (13 D) were found to be strongly different, with that of DMABN-F4 being anomalously low. On the other hand, the calculations indicate that the dipole moments should be similar (16.7 and 16.8 D, respectively, Table 11), and the transient absorption experiments[19] also indicate that the electronic structure is similar and full charge separation has occurred.

This discrepancy is solved if the assumption of equal Onsager radii a is dropped, because the solvatochromic slope is proportional to the ratio μ_e/a^3. An increased a for DMABN-F4 will lead to a correspondingly increased μ_e. In fact, we can estimate that an increase from $a = 3.7$ to $a = 5.3$ is necessary to result in similar dipole moments for the TICT states of both DMABN and DMABN-F4. On the other hand, using the molecular volumes estimated by quantum chemical calculations and from the densities and molecular weights (Table 8), we concluded that the solvent cavity volume excluded by the solvent should be very similar for the two compounds. Using Onsager's point dipole approximation, which is at the basis of the solvatochromic treatment according to Mataga, we are therefore forced to conclude for different CT dipole moments from the different experimental solvatochromic slopes.

A possibility for justifying differently sized a-factors for the two compounds would be by assuming different solute−solvent interactions for the same excluded volume of the solvent (directly related to the a-factor) in Onsager theory. If the solute−solvent response would be weaker in DMABN-F4 than that in DMABN, this would correspond to an increased a-factor in the usual solvatochromic equation. This is equivalent to say that the Onsager point dipole approximation is not valid for this comparison.

We can justify such a point of view by considering the different charge distribution in the two compounds: Starting from the transient absorption experiments,[19] we can conclude that there is full charge separation in the CT state of both compounds. Especially the signature of the radical anion of the benzonitrile acceptor is seen in both cases. The π and π^* orbitals are very similar for the two compounds (see the calculations, Table 11); hence the charge distribution due to the π-electronic transitions should be similar in the CT states of the two compounds. The fluorine atoms on the acceptor are negatively charged (in both ground and excited state), however, whereas the H-atoms in DMABN are positively charged. The negative charge on the fluorine atoms will prepolarize the solvent dipoles already in the ground state such that upon excitation to the charge-transfer state, their relaxation possibility is reduced, which is equivalent to say that the solute−solvent interaction is effectively weakened.

This explanation of the dipole moment discrepancy by a breakdown of the Onsager point dipole theory is a first attempt to explain the unusual solvatochromic behavior of highly fluorinated charge-transfer compounds. Further experiments are needed to verify this explanation.

3.8. Competing Photochemical Reaction Paths. The value of k_{nr} is considerably larger for DMABN-F4 than that for DMABN, especially in *n*-hexane (Table 3). We can conclude that we have an additional nonradiative decay channel: Its nature could be either population of a triplet state (intersystem crossing ISC) or population of a transient nonemissive singlet species and/or nonradiative photochemistry through a conical intersection (internal conversion IC). Because there is no permanent photochemical product, these reaction paths have to lead back to the ground state of the starting material. Because we do not observe phosphorescence, the triplet path is not probable. The number of fluorine substituents seems to be an important factor in the enhancement of this IC path as already stated by Zachariasse et al.[7] In the tetrafluorinated DMABN, this IC path is further enhanced as compared with the monofluorinated derivatives.

A possible reaction path that can be discussed is the folding (relaxation to nonplanarity) of the benzene ring in the excited state. Recent calculations of DMABN indicate that, even in this nonfluorinated compound, the TICT state possesses a nonplanar benzene ring.[23] The case of 1,2,4,5-tetrafluorobenzene further exemplifies the effect of the fluorine atoms that enhances the tendency for nonplanar folding: Whereas benzene shows no sign of a deviation from planarity in the emissive excited state, the emissive state of tetrafluorobenzene shows a folding (butterfly motion) resulting in a double minimum potential, as deduced from laser-induced fluorescence spectra.[24] If there is a similar folding in DMABN-F4 (and to some extent even in DMABN, which also has a nonnegligible contribution of IC[25] with k_{ic} of 8.64×10^7 S^{1-} in acetonitrile solvent), it could lead to a conical intersection along the reaction coordinate leading either to the Dewar isomer (folding of two four-membered rings) or to the benzvalene isomer (folding of two three-membered rings). Such conical intersections are known to play an important role in the nonradiative photochemistry of benzene and its derivatives.[26−28]

4. Conclusion

DMABN-F4 is spectroscopically closely related to DMABN but characterized by a higher acceptor strength of the benzonitrile moiety. The strongly red-shifted emission and absence of the short wavelength B-band in the fluorescence spectrum of DMABN-F4 at 77 K indicates the ultrafast formation of a CT structure in the excited state, probably linked to the pretwisted ground-state geometry due to the sterical hindrance by the fluorine atoms[29] and the increased acceptor strength. The low fluorescence quantum yield values and absence of phosphorescence of DMABN-F4 suggest that the high rate of nonradiative decay takes place through internal conversion rather than intersystem crossing. A possible intersystem crossing reaction path could be the folding (butterfly motion) of the benzene ring toward either a Dewar or a prefulvene deformation. Results from time-resolved measurements indicate that the emission of DMABN-F4 is strongly forbidden, consistent with the formation of a TICT state with high dipole moment. The relatively small solvatochromic slope for this CT emission, as compared to expectations from quantum chemical calculations, indicates the possibility for a breakdown of the Onsager point dipole approximation for highly fluorinated CT compounds.

References and Notes

(1) Lippert, E.; Lüder, W.; Boos, H. *Adv. Mol. Spectrosc. Proc. Int. Meet. 4th* **1959**, 443.

(2) Grabowski, Z. R.; Rotkiewicz, K.; Siemiarczuk, A.; Cowley, D. J.; Baumann, W. *Nouv. J. Chim.* **1979**, *3*, 443.

(3) Rettig, W. *Angew. Chem., Int. Ed. Engl.* **1986**, *25*, 971.

(4) Rettig, W. *Top. Curr. Chem.* **1994**, *169*, 253.

(5) Grabowski, Z. R.; Rotkiewicz, K.; Rettig, W. *Chem. Rev.* **2003**, *103*, 3899.

(6) (a)Wermuth, G. *Z. Naturforsch.* **1983**, *38a*, 641 (b) Schuddeboom, W.; Jonker, S. J.; Warman, J. M.; Leinhos, U.; Kühnle, W.; Zachariasse, K. A. *J. Phys. Chem.* **1992**, 96, 10809.

(7) Druzhinin, S. I.; Jiang, Y. B.; Demeter, A.; Zachariasse, K. A. *Phys. Chem. Chem. Phys.* **2001**, *3*, 5213.

(8) Felstead, E.; Fielding, H. C.; Wakefield, B. J. *J. Chem. Soc. C* **1966**, *7*, 708.

(9) (a) Meech, S. R.; Phillips, D. *J. Photochem.* **1983**, *23*, 193. (b) Velapoldi, R. A.; Epstein, M. S. In *Luminescence Applications in Biological, Chemical, Environmental, and Hydrological Sciences*; Goldberg, M. C., Ed.; ACS Symposium Series 383; American Chemical Society: Washington, DC, 1989; p98.

(10) Riddick, J. A.; Bunger, W. A.; Sakano, T. K. *Organic Solvents*, 4th ed.; Techniques of Chemistry, Vol. II; Wiley: New York, 1986.

(11) O'Connor, D. V.; Phillips, D. *Time Correlated Single Photon Counting*; Academic Press: London, 1984.

(12) Weigel, W.; Rettig, W.; Dekhtyar, M.; Modrakowski, C.; Beinhoff, M.; Schlüter, D. *J. Phys. Chem.* **2003**, *107*, 5941.

(13) Dewar, M. J. S.; Zoeblich, E. G.; Healy, E. F.; Stewart, J. J. P. *J. Am. Chem. Soc.* **1985**, *107*, 3202.

(14) *AMPAC 6.0* and *AMPAC 6.55*; Semichem, Inc.: Shawnee Mission, KS, 1997.

(15) Frisch, M. J.; Trucks, G. W.; Schlegel, H. B.; Gill, P. M. W.; Johnson, B. G.; Robb, M. A.; Cheeseman, J. R.; Keith, T.; Petersson, G. A.; Montgomery, J. A.; Raghavachari, K.; Al-Laham, M. A.; Zakrzewski, V. G.; Ortiz, J. V.; Foresman, J. B.; Cioslowski, J.; Stefanov, B. B.; Nanayakkara, A.; Challacombe, M.; Peng, C. Y.; Ayala, P. Y.; Chen, W.; Wong, M. W.; Andres, J. L.; Replogle, E. S.; Gomperts, R.; Martin, R. L.; Fox, D. J.; Binkley, J. S.; Defrees, D. J.; Baker, J.; Stewart, J. P.; Head-Gordon, M.; Gonzalez, C.; Pople, J. A. *Gaussian 98*, revision A.7; Gaussian, Inc.: Pittsburgh, PA, 1998.

(16) Rettig, W.; Braun, D.; Suppan, P.; Vauthey, E.; Rotkiewicz, K.; Luboradzki, R.; Suwińska, K. *J. Phys. Chem.* **1993**, *97*, 13500.

(17) Grabowski, Z. R.; Rotkiewicz, K.; Rubaszewska, W.; Kirkor-Kamińska, E. *Acta Phys. Pol., A* **1978**, *54*, 767.

(18) Rotkiewicz, K.; Rubaszewska, W. *J. Lumin.* **1982**, *27*, 221.

(19) Murali, S.; Changenet-Barret, P.; Ley, C.; Plaza, P.; Rettig, W.; Martin, M. M.; Tolmachev, A. I. In *Femtochemistry and Femtobiology: Ultrafast Events in Molecular Science*; VIth International Conference on Femtochemistry, Maison de la Chimie, Paris, France, July 6−10, 2003; Martin, M., Hynes, J. T., Eds.; Elsevier: Amsterdam, 2004; p 323.

(20) Köhler, G.; Rotkiewicz, K. *Spectrochim. Acta, Part A* **1986**, *42*, 1127.

(21) (a) Lippert, E. *Z. Naturforsch., A: Phys. Sci.* **1955**, *10*, 541. (b) Mataga, N.; Kaifu, Y.; Kazumi, M. *Bull. Chem. Soc. Jpn.* **1955**, 28, 690; **1956**, *29*, 465.

(22) Rösch, N.; Zerner, M. C. *J. Phys. Chem.* **1994**, *98*, 5817.

(23) Köhn, A.; Hättig, C. *J. Am. Chem. Soc.* **2004**, *126*, 7399.

(24) Okuyama, K.; Kakinuma, T.; Fujii, M.; Mikami, N.; Ito, M. *J. Phys. Chem.* **1986**, *90*, 3948.

(25) Chattopadhyay, N.; Rommens, J.; Van der Auweraer, M.; De Schryver, F. C. *Chem. Phys. Lett.* **1997** *279*, 303.

(26) Tsuda, M.; Oikawa, S.; Kimura, K. *Int. J. Quantum Chem.* **1980**, *18*, 157.

(27) Kato, S. *J. Chem. Phys.* **1988**, *88*, 3045.

(28) Sobolewski, A. L.; Woywod, C.; Domcke, W. *J. Chem. Phys.* **1993**, *98*, 5627.

(29) (a) Rajnikant; Watkin, D.; Trunter, G. *Acta Crystallogr., Sect. C* **1995**, *51*, 1452. (b) Grein, F. *J. Phys. Chem. A* **2002**, *106*, 3823.